JOURNAL OF SOLID STATE CHEMISTRY 53, 184–192 (1984)

A Pentagonal Tunnel Structure with Copper in Square Planar Coordination: The Oxides $KCuNb_3O_9$ and $KCuTa_3O_9$

D. GROULT, M. HERVIEU, AND B. RAVEAU

Laboratoire de Cristallographie, Chimie et Physique des Solides, L.A. 251, ISMRA-Université, 14032 Caen Cedex, France

Received September 15, 1983; in revised form December 30, 1983

The structure of two new oxides $KCuTa_3O_9$ and $KCuNb_3O_9$ has been solved from X-ray powder data and by electron microscopy. Both compounds are orthorhombic, space group $Pnc2$ with $a \simeq 8.8$ Å, $b \simeq 10.1$ Å, and $c \simeq 7.6$ Å. Their host lattice is built up from corner-sharing MO_6 octahedra (M = Nb, Ta) forming pentagonal tunnels where the K^+ ions are located. The copper ions are located in distorted perovskite $CaCu_3Mn_4O_{12}$-type cages and exhibit a square planar coordination. The relationships between these oxides and the TTB, HTB, ITB, and $Ba_{0.15}WO_3$ structures are discussed.

Introduction

As a part of a study of the AMO_3–CuM_2O_6 systems, oxides with the general formula $ACu_3M_7O_{21}$ (A = K, Rb, Cs, Tl; M = Ta, Nb) have been isolated (*1*). Their structure was found to be built up from hexagonal tungsten bronze slabs "AM_3O_9" and perovskite-like slabs "$Cu_3M_4O_{12}$" in which copper exhibits the square planar coordination. These phases were described as the 1 : 1 member of a series of intergrowths corresponding to the formulation $(AM_3O_9)_n(Cu_3M_4O_{12})_{n'}$. The systems involving potassium exhibit a particular behavior. For the molar ration KMO_3: CuM_2O_6 = 1, a new phase has been observed. It crystallizes in the orthorhombic system with unit cell dimensions very close to that of the barium tungsten bronze $Ba_{0.15}WO_3$ (*2*) studied in the laboratory. We report here the structural study of the oxides $KCuTa_3O_9$ and $KCuNb_3O_9$, and their relationships with the HTB (*3, 4*), TTB (*5–7*), and ITB (*8–11*) structures.

Experimental

The two compounds were synthesized in air, in platinum crucibles, from mixtures of the tantalates and niobates KMO_3 and CuM_2O_6 (M = Ta, Nb) previously prepared by solid state reaction between K_2CO_3 and the M_2O_5 (M = Ta, Nb) and CuO.

The mixtures were first heated 12 hr at 900°C, quenched, and then annealed at 1000°C during 24 hr. The final compounds were characterized by their X-ray diffractograms using a Philips goniometer with Cu$K\alpha$ radiation.

ESR measurements were recorded from a BRÜKER, E 200 X-band spectrometer equipped with a double cavity which can give simultaneously the pattern of the sample and of a standard (strong pitch g = 2.0028). The densities were measured at 20°C by picnometry in CCl_4.

For the electron microscopy observations, niobate samples were ground in an agate mortar. After being dispersed in n-butanol, the small particles were collected

0022-4596/84 $3.00

TABLE I

UNIT CELL DIMENSIONS OF THE OXIDES $KCuTa_3O_9$ AND $KCuNb_3O_9$

Molecular formula	a (Å)	b (Å)	c (Å)	d obs. (g/cm^3)	d calc. (g/cm^3)
$KCuTa_3O_9$	8.862(8)	10.187(10)	7.638(6)	7.62(6)	7.57
$KCuNb_3O_9$	8.823(5)	10.144(5)	7.683(4)	5.12(5)	5.07

on a copper-supported holey carbon film. Observations were made with a JEOL 100 CX microscope operating at 120 kV. Electron diffraction study was carried out with a goniometer stage (±60°) and lattice images were obtained with a top-entry goniometer and a high resolution objective lens with a spherical aberration constant of 0.7 mm. All images were recorded by using an objective aperture with a radius of 0.42 Å^{-1} in reciprocal space. Through-focus series of images were calculated with two programs, F. COEFF and DEFECT, developed by Skarnulis (*12*) with incident beam convergency $\alpha = 0.6$ mrad and defocus spread $D = 200$ Å.

Results

Both oxides $KCuTa_3O_9$ and $KCuNb_3O_9$ are obtained in the form of well-cristallized powders, green for the tantalate and brown for the niobate. The electron diffraction study of $KCuNb_3O_9$ showed an orthorhombic symmetry with the reflection conditions $(0kl)$ $k + l = 2n$ and $(h0l)$ $l = 2n$ indicating possible space groups *Pncm* or *Pnc*2. Because a second harmonic generation acentricity test was positive, the latter group has been retained for the refinement of the structure. The X-ray diffraction patterns were indexed in this orthorhombic cell with the refined parameters listed in Table I. The observed densities show four formula units per cell.

The ESR patterns of the two compounds, registered at 300 and 77 K, appear furthermore identical to that of the oxides $CuTa_2O_6$, $CaCu_3Ti_4O_{12}$, and $Cu_3Ta_2Ti_2O_{12}$ studied by Propach (*13*). Consequently, owing to the g and ΔH values observed ($g = 2.167$, $\Delta H_{pp} = 250$ G at 77 K) one may assume that the copper ions may be located in strongly distorted sites, surrounded by 12 oxygens.

Structure Solution and Refinement

No single crystals could be obtained for either compound. The structure was therefore solved from X-ray powder data of the tantalate $KCuTa_3O_9$.

The heavy atom positions were deduced from a Patterson section perpendicular to the c axis, using the first 25 independent intensities corrected for PLG and multiplicity. This allowed us to place the Ta atoms on the 4(c) sites of the acentric group *Pnc*2 and showed without ambiguity the presence of triangular units with Ta–Ta distances close to 3.8 Å. Such units which may be formulated Ta_3O_{15} if one assumes an octahedral oxygen environment for the Ta atoms, form the structural units of several oxides $A_xM_xM'_{1-x}O_3$ ($0 \leq x \leq 1$) with TTB-, HTB-, and ITB-like structures.

The comparison of the cell-dimensions of the tantalate $KCuTa_3O_9$ with that of $Ca_2TlTa_5O_{15}$ (*14*) and TTB compounds leads to the relations

$$a_{KCuTa_3O_9} \simeq a_{TTB}\sqrt{2}/2$$
$$b_{KCuTa_3O_9} \simeq b_{Ca_2TlTa_5O_{15}}$$
$$c_{KCuTa_3O_9} \simeq c_{TTB} \times 2 \simeq c_{Ca_2TlTa_5O_{15}} \times 2$$

This suggested the structural model shown in Fig. 1.

In order to verify this hypothesis, structure factor calculations were carried out from the 42 observed reflections, i.e., 152 *hkl*. The atomic scattering factors used were those of Cromer and Waber corrected for anomalous dispersion. Three sets of Ta atoms were located on the 4(c) sites, the K^+ ions were located on a 4(c) site (x, y, z) in-

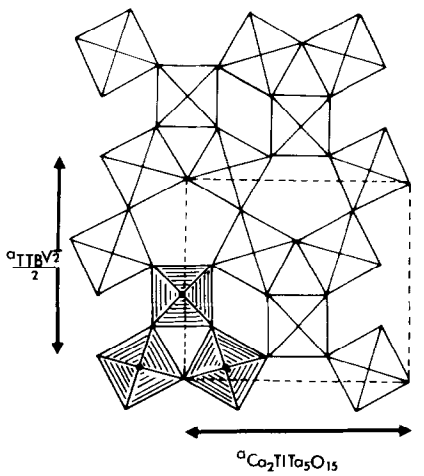

FIG. 1. Idealized model of the M_6O_{18} framework showing the relation parameters with the TTB and $Ca_2TlTa_5O_{15}$ compounds.

side the pentagonal tunnel and the Cu^{2+} ions on two 2(*b*) sites ($\frac{1}{2}$, 0, *z*) within the perovskite sites. The oxygen atoms were distributed on 4(*c*) and 2(*a*) sites with respect to the octahedral surrounding of the Ta atoms. Owing to the number of powder data available, the thermal parameters were not refined, but were fixed at 0.3 Å^2 for the metallic atoms and 1 Å^2 for the oxygen atoms. Refinements of the atomic coordinates were carried out on intensities taking into account the overlapping reflections according to Ref. (*17*). The discrepancy factor $R_I = \Sigma|I_0 - I_c|/\Sigma I_0$ was first lowered to 0.18 by refining the Ta positions. It was reduced to 0.10 by refining the atomic parameters of K^+ and Cu^{2+} ions and finally to a rather low value equal to 0.067 by refining the atomic coordinates of the oxygen atoms. Final atomic parameters with their estimated standard deviations in parentheses are given in Table II. The observed and calculated values of the intensities have been listed in Table III. On account of the great number of variable parameters versus the rather low number of reflections, it is obvious that this structure can only be considered as a model and especially that the oxygen positions are not known with accuracy. Nevertheless, refinement in the centrosymmetric space group *Pncm* which has one-half the variable parameters gave very similar atomic coordinates and discrepancy factor ($R_I = 0.07$). However, the use of this latter group requires splitting some oxygen positions with an occupancy factor of 0.5 in order to obtain correct Cu–O distances. Moreover, it appears that these split positions coincide with those observed for the oxygen atoms O(8), O(9), and O(10) of the non-centrosymmetrical space group *Pnc*2 (Table II) in agreement with the results of the SHG acentricity test.

Selected interatomic distances are listed in Table IV and the numbering scheme used shown in Fig. 2. Similar results have been obtained for $KCuNb_3O_9$ ($R_I = 0.062$).

High Resolution Microscopy Study

Experimental images of tantalate single-crystal fragments could not be obtained owing to their darkness.

Although they were ground under liquid nitrogen, the niobate samples appeared to be relatively thick and the crystal flakes,

TABLE II

FINAL ATOMIC PARAMETERS WITH esd's IN PARENTHESES FOR $KCuTa_3O_9$

Atom	Position	*x*	*y*	*z*	*B* (Å)
K	4(*c*)	0.081(4)	0.259(6)	0.255(9)	0.3
Cu(1)	2(*b*)	$\frac{1}{2}$	0	0.252(8)	0.3
Cu(2)	2(*b*)	$\frac{1}{2}$	0	0.752(4)	0.3
Ta(1)	4(*c*)	0.4292(11)	0.252(5)	−0.003(8)	0.3
Ta(2)	4(*c*)	0.8021(15)	0.4360(11)	−0.018(5)	0.3
Ta(3)	4(*c*)	0.7991(15)	0.0613(11)	−0.012(9)	0.3
O(1)	2(*a*)	0	0	0.0	1.0
O(2)	2(*a*)	0	0	0.5	1.0
O(3)	4(*c*)	0.260(8)	0.118(8)	−0.031(9)	1.0
O(4)	4(*c*)	0.259(8)	0.403(8)	0.061(8)	1.0
O(5)	4(*c*)	0.575(7)	0.384(8)	0.058(9)	1.0
O(6)	4(*c*)	0.576(8)	0.392(7)	0.461(8)	1.0
O(7)	4(*c*)	0.875(8)	0.253(8)	0.006(9)	1.0
O(8)	4(*c*)	0.406(8)	0.186(8)	0.258(9)	1.0
O(9)	4(*c*)	0.171(9)	0.589(10)	0.249(8)	1.0
O(10)	4(*c*)	0.271(9)	0.540(11)	0.757(9)	1.0

TABLE III

RETICULAR DISTANCES AND INTENSITIES OBSERVED AND CALCULATED FOR $KCuTa_3O_9$

h k l	*d* obs.	*d* calc.	*I* obs.	*I* calc.	*h k l*	*d* obs.	*d* calc.	*I* obs.	*I* calc.
1 0 0	8.90	8.862	15.47	19.02	5 0 0	1.771	1.7724	5.13	7.34
1 1 0	6.70	6.686	3.20	2.95	1 4 3		1.7645		0.08
0 2 0	5.09	5.093	8.46	11.19	1 5 2	1.757	1.7617	18.38	11.19
2 0 0	4.41	4.431	29.91	5.19	2 0 4		1.7536		1.41
1 2 0		4.416		19.84	1 2 4	—	1.7526		4.23
2 1 0	4.06	4.063	35.81	35.71	5 1 0	—	1.7461		3.05
1 2 1	3.822	3.823	78.12	0.03	2 1 4	1.726	1.7281	7.80	7.55
0 0 2		3.819		77.68	3 4 2	—	1.7217		0.03
2 2 0	3.342	3.343	47.00	41.66	5 1 1	—	1.7022	6.92	0.00
1 1 2	3.316	3.316		5.81	0 6 0	1.696	1.6978		7.69
1 3 0	3.168	3.170	85.98	78.11	3 5 0	1.675	1.6771	94.44	13.26
3 0 0	2.954	2.954	31.28	30.49	3 3 3	—	1.6769		0.02
1 3 1	2.888	2.9285	100.00	0.26	5 2 0	—	1.6739		1.25
2 0 2		2.8886		20.38	4 4 0	—	1.6715		0.00
1 2 2		2.8928		80.27	4 3 2	1.669	1.6682		43.39
3 1 0	2.837	2.8371	21.96	22.75	2 4 3	—	1.6681		0.38
2 1 2	2.783	2.7828	35.90	37.35	1 6 0	—	1.6675		0.01
3 2 0	2.552	2.5553	21.71	10.97	2 5 2	1.662	1.6657		22.76
0 4 0	2.543	2.5467		8.42	2 2 4		1.6580		11.15
2 3 1		2.5416		0.22	3 5 1	—	1.6381	22.05	0.02
2 2 2	2.514	2.5154	54.36	50.39	1 3 4	1.633	1.6358		24.51
1 4 0	—	2.4476	50.51	4.02	5 2 1	—	1.6351		0.07
1 3 2	2.436	2.4395		44.58	4 4 1	—	1.6328		0.04
3 2 1	—	2.4233		0.67	1 6 1	—	1.6291		0.14
3 0 2	2.336	2.3365	13.50	13.36	5 0 2	1.605	1.6077	33.16	20.98
1 4 1		2.3309		0.14	3 0 4	1.602	1.6036		10.11
3 1 2	2.276	2.2774	7.35	7.45	0 5 3	—	1.5907	15.13	0.01
4 0 0	—	2.2155	8.97	1.57	5 1 2	—	1.5880		2.15
1 4 0	2.204	2.2080		9.04	4 2 3	—	1.5880		0.04
1 2 3		2.2056		0.47	2 6 0	—	1.5854		1.77
2 3 2	—	2.2020		0.54	3 1 4	1.584	1.5841		10.13
0 3 3	2.031	2.0370	7.60	0.10	2 6 1	1.548	1.5523	10.52	0.05
4 2 0		2.0316		8.71	0 6 2		1.5514		13.40
2 2 3		2.0255		0.22	5 3 1		1.5390		0.06
1 5 0	1.984	1.9856	8.72	8.35	3 4 3	—	1.5374	30.26	0.10
1 3 3		1.9852		0.20	3 5 2	1.534	1.5356		12.05
0 5 1		1.9685		0.16	5 2 2	—	1.5331		5.08
2 4 2	1.908	1.9115	30.34	0.69	4 4 2	—	1.5312		1.17
0 0 4		1.9095		30.41	3 2 4	—	1.5296		4.90
3 1 3		1.8949		0.31	1 6 2	1.528	1.5281		4.60
4 3 0	1.853	1.8554	37.26	26.11	0 4 4	—	1.5277		4.48
2 5 0		1.8510		10.57					
2 3 3		1.8508		0.01					

TABLE IV

SELECTED INTERATOMIC DISTANCES (Å) FOR $KCuTa_3O_9$

Ta-octahedra		Cu-polyhedra	
Ta(1)–O(3)	2.04(7)	Cu(1)–O(8)	2.07(8) × 2
Ta(1)–O(4)	2.20(8)	Cu(1)–O(10)	2.07(8) × 2
Ta(1)–O(5)	1.92(7)	Cu(1)–O(5)	2.70(9) × 2
Ta(1)–O(6)	1.99(7)	Cu(1)–O(6)	2.58(8) × 2
Ta(1)–O(8)	2.11(9)	Cu(1)–O(3)	3.26(8) × 2
Ta(1)–O(8)	1.93(9)	Cu(1)–O(4)	3.32(8) × 2
⟨Ta(1)–O⟩	2.03(8)		
Ta(2)–O(2)	1.88(1)	Cu(2)–O(5)	2.01(8) × 2
Ta(2)–O(4)	1.83(8)	Cu(2)–O(6)	2.05(7) × 2
Ta(2)–O(5)	2.15(7)	Cu(2)–O(4)	2.77(7) × 2
Ta(2)–O(7)	1.98(8)	Cu(2)–O(3)	2.95(7) × 2
Ta(2)–O(9)	2.07(7)	Cu(2)–O(8)	3.30(8) × 2
Ta(2)–O(10)	1.85(8)	Cu(2)–O(9)	3.05(8) × 2
⟨Ta(2)–O⟩	1.96(6)		
Ta(3)–O(1)	1.89(1)	K-polyhedron	
Ta(3)–O(3)	1.90(7)		
Ta(3)–O(6)	2.04(6)	K–O(3)	2.60(9)
Ta(3)–O(7)	2.07(8)	K–O(4)	2.61(9)
Ta(3)–O(10)	2.16(9)	K–O(7)	2.64(9)
Ta(3)–O(9)	1.87(9)	K–O(7)	2.65(9)
⟨Ta(3)–O⟩	1.99(6)	K–O(9)	2.71(8)
		K–O(8)	2.97(9)
		K–O(3)	3.06(9)
		K–O(1)	3.15(6)
		K–O(2)	3.20(6)
		K–O(4)	3.25(10)

overlapping holes in the carbon films, were tilted into the (001) zone. The images at relatively low magnification show the perfection of the crystals. In the bulk of the crystals, the image contrast appears as white spots forming lines with about 8.8-Å spacings in the "*a*" direction. Figure 3 shows such a micrograph for $KCuNb_3O_9$ with (001) incidence. In these crystals, no defects similar to those encountered in the isotypic compound $Ba_{0.15}WO_3$ (*2*) are observed. This feature is certainly due to the occupancy of the rhombic tunnels by the copper ions which avoid the formation of the chemical twin defects. The contrast being very sensitive to the crystal thickness, only the thinnest edges of the crystals gave high resolution and thus, two characteristic

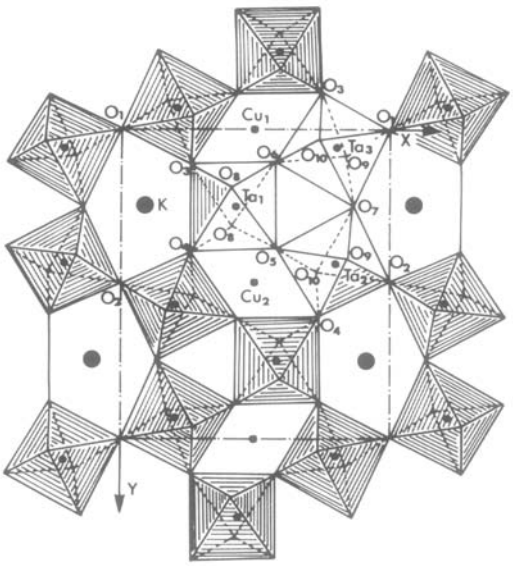

FIG. 2. Projection of the structure of $KCuTa_3O_9$ on to (001).

types of images were frequently observed. They are shown in Figs. 4a and b.

Simulations were carried out for many crystal thicknesses and focus values, using the structural model deduced from X-ray diffraction data for $KCuNb_3O_9$. For a crystal thickness of 38 Å, it was found that the calculated images are similar to those observed on the thin edges.

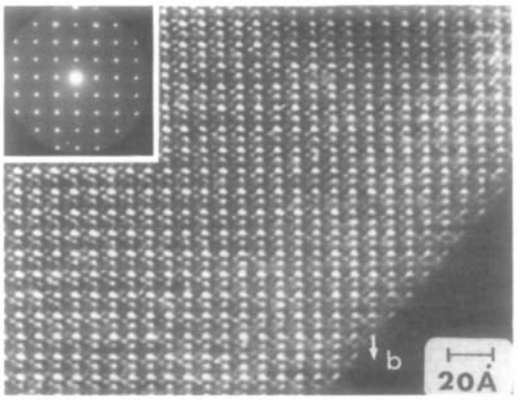

FIG. 3. Electron micrograph (001) image of a thick part of $KCuNb_3O_9$ with an inset diffraction pattern.

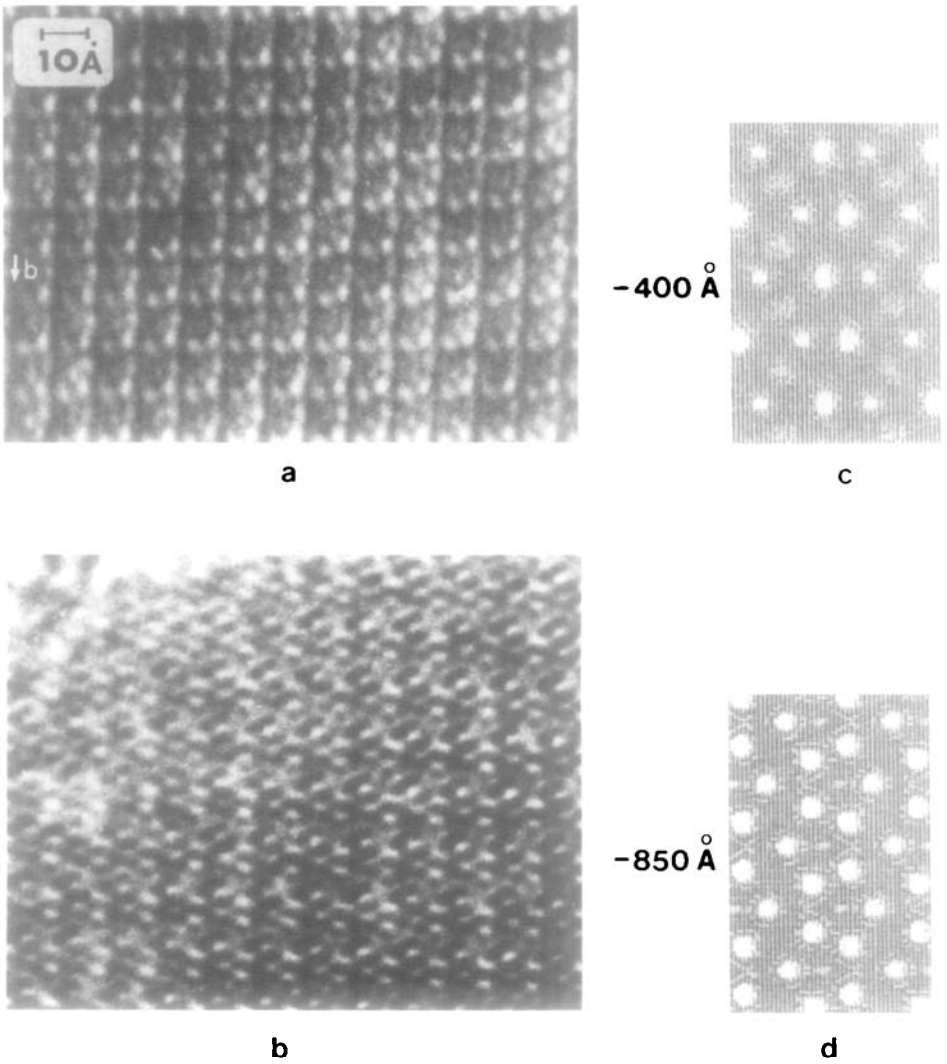

FIG. 4. Comparison of the experimental images (a, b) taken from the thin edge with calculated images (2×2 unit cells) for the (001) zone of the niobate $KCuNb_3O_9$ (thickness $\sim$ 38 Å—undefocus: (c) -400 Å, (d) -850 Å).

These images, for -400 and -800 Å defocus values, are shown in Figs. 4c and d. The zigzag ribbons of the whitest spots of Fig. 4a correspond to the positions of the pentagonal tunnels while the weakest ones correspond to the small triangular tunnels. The contrast of the Fig. 4b appears as approximatively reversed. Uneven contrasts suggest that in some areas of the crystallites, the filling of the pentagonal tunnels by K^+ ions is irregular but no superlattice spots have been observed in the (*hk0*) electron diffraction patterns. However, during the electron diffraction study, some diffraction patterns down the *b* axis, indicated tripling along the "*a*" direction as shown in

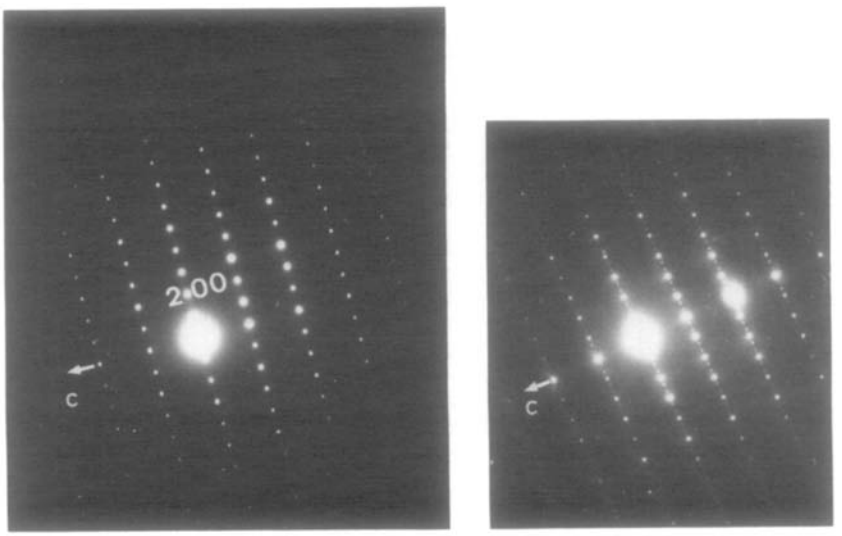

FIG. 5. Electron diffraction patterns recorded with the electron beam parallel to $\vec{b}$ from $KCuNb_3O_9$ fragment crystallites: (a) corresponding to the X-ray unit cell, (b) encountered superlattice pattern.

Fig. 5. This could be due to an ordering of K^+ ions which would exhibit a slight deviation from stoichiometry.

Description of the Structure

The structure of $KCuTa_3O_9$ and $KCuNb_3O_9$ contains an assemblage of corner-sharing TaO_6 or NbO_6 octahedra very similar to that observed for the tungsten bronze $Ba_{0.15}WO_3$ (*2*), and forming three sorts of tunnels: pentagonal, rhombic, and triangular. However, contrary to $Ba_{0.15}WO_3$, the pentagonal tunnels are fully occupied by K^+ ions while the rhombic tunnels, which are empty in $Ba_{0.15}WO_3$, are fully occupied by Cu^{2+} ions. Moreover, this structure differs from that of the barium bronze by the tilting of the MO_6 octahedra (M = Ta, Nb). They are indeed tilted with respect to each other in the [001] direction, the angle of the tilt being greater in the case of the Ta(1)–O_6 octahedron than in the Ta(2)–O_6 and Ta(3)–O_6 octahedra, namely 19° compared to 15°. A similar behavior has been reported for several copper oxides with the perovskite structure, $CaCu_3M_4O_{12}$ (M = Ti, Mn), in which the angle of the tilt was found close to 20°. Such a distortion results from the Jahn–Teller effect of the Cu^{2+} ions which stabilize the octahedral tilting and consequently the structure. Thus the Ta(1)–O_6 octahedron which is surrounded by two Cu^{2+} ions and one K^+ ion appears more tilted than the Ta(2)–O_6 and Ta(3)–O_6 octahedra which are surrounded by one Cu^{2+} ion and two K^+ ions.

The Ta atoms are slightly displaced from the center of the octahedra and exhibit three Ta–O distances close to 2.10 Å and three shorter distances close to 1.90 Å. The mean Ta–O distance in the three octahedra are 2.03(8) Å for Ta(1), 1.96(6) Å for Ta(2), and 1.99(6) Å for Ta(3) which may be compared with the average distance of 1.97 Å in $K_6Ta_{10.8}O_{30}$ (*18*) and 1.98(5) Å in $CuTa_2O_6$ (*16*).

The K^+ ions are located inside the pentagonal prismatic tunnel with eight nearest-neighbor oxygen atoms at distances which range from 2.60 to 3.15 Å (mean 2.80 Å) and

seven oxygen atoms at distances which range from 3.20 to 3.83 Å and cannot be considered, indeed, as bonded K–O distances. Owing to the tilting of the octahedral framework, the K^+ polyhedron is more distorted than, for example, in the TTB tantalate $K_6Ta_{10.8}O_{30}$ (*18*) which shows a regular tricapped trigonal prism for K^+ ions in the A(2) site.

The Jahn–Teller cations Cu^{2+} are surrounded by 12 oxygen atoms arranged as three unequal perpendicular rectangles which lead to three sets of Cu–O distances. From the values which have been listed in Table IV it is clear that the copper ions exhibit a square coordination with four Cu–O distances close to 2 Å as previously found for the tantalates $CuTa_2O_6$ (*16*), $RbCu_3Ta_7O_{21}$ (*1*), and the perovskites $CaCu_3M_4O_{12}$ (M = Ti, Mn) (*19*).

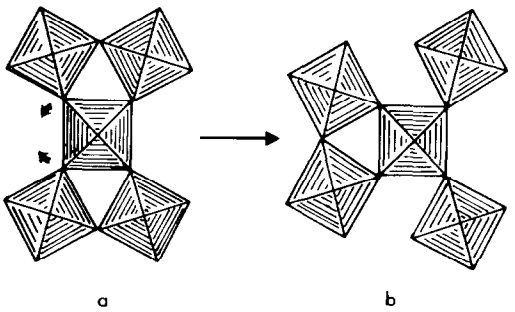

FIG. 6. Relations between the M_5O_{15} units used to describe the structures (a) of the HTB, TTB, and ITB oxides, (b) of the tantalate and niobate $KCuM_3O_9$ (M = Ta, Nb).

Discussion

The structure is closely related to the TTB type and to the distorted perovskite $CaCu_3Mn_4O_{12}$. One, indeed, observes pentagonal rings built up of five corner-sharing octahedra, joined together along the [100] and [001] directions by sharing the corners of their octahedra and along the [010] direction by having two common octahedra in such a way that two successive pentagonal rings share one corner in this direction. The structure may also be described as built up from M_5O_{15} units (M = Ta, Nb) derived from the structural units of HTB, TTB, and ITB bronzes by a rotation of 60° of two apical octahedra as shown on the Fig. 6. The assemblage of these basic units by common octahedra in the [010] direction leads to perovskite sites with a rhombic section similar indeed with the situation observed in ITB oxides but different from that described for the TTB compounds which exhibit tetragonal sites with a square section. As a result, these types of sites may accommodate Cu^{2+} ions as previously shown for the distorted perovskites $CaCu_3M_4O_{12}$ (M = Ti, Mn) (*19*) and the ITB oxides $ACu_3M_7O_{21}$ (*1*) (M = Nb, Ta).

By assuming a square coordination, the Cu^{2+} ions are responsible for the tilting of the oxygen network which appears more regular in the barium tungsten bronze $Ba_{0.15}WO_3$ in which the rhombic sites are empty. Furthermore it is worthy of note that the full occupation of the perovskite sites by copper ions and the pentagonal tunnels by K^+ ions leads to a structure without defects while chemical twin defects have been observed in $Ba_{0.15}WO_3$ (*2*).

In spite of the presence of pentagonal tunnels, this structure appears as very closely related to the ITB $Ca_2TlTa_5O_{15}$ (*14*). Both structures contain identical rows of corner-sharing octahedra running along the b axis for the former and along the a axis for the latter. Therefore, it appears that the possibility of formation of intergrowths between the two structures should be investigated.

Acknowledgments

The authors thank F. Huard (Laboratoire de Chimie Minérale Appliquée, Montpellier) for doing the S.H.G. acentricity experiment.

References

1. A. Benmoussa, D. Groult, F. Studer, and B. Raveau, *J. Solid State Chem.* **41,** 221 (1982).
2. C. Michel, M. Hervieu, R. J. D. Tilley, and B. Raveau, *J. Solid State Chem.* **52,** 281 (1984).
3. A. Magneli and B. Blomberg, *Acta Chem. Scand.* **5,** 372 (1951).
4. A. Magneli, *Acta Chem. Scand.* **7,** 315 (1953).
5. A. Magneli, *Ark. Kemi* **1,** 213 (1949).
6. F. Takusagawa and R. A. Jacobson, *J. Solid State Chem.* **18,** 163 (1976).
7. L. Kihlborg and A. Klug, *Chem. Scr.* **3,** 207 (1973).
8. A. Hussain and L. Kihlborg, *Acta Crystallogr. Sect. A* **32,** 551 (1976).
9. A. Hussain, *Chem. Scr.* **11,** 224 (1977).
10. L. Kihlborg, M. Sundberg, and H. Hussain, *Chem. Scr.* **15,** 182 (1980).
11. L. Kihlborg and R. Sharma, *J. Microsc. Spectrosc. Electron.* **7,** 387 (1982).
12. A. J. Skarnulis, E. Summerville, and L. Eyring, *J. Solid State Chem.* **23,** 59 (1978).
13. V. Propach, *Z. Anorg. Allg. Chem.* **435,** 161 (1977).
14. M. Ganne, M. Dion, A. Verbaere, and M. Tournoux, *J. Solid State Chem.* **29,** 9 (1979).
15. J. Chenavas, J. C. Joubert, M. Marezio, and B. Bochu, *J. Solid State Chem.* **14,** 25 (1975).
16. H. Vincent, B. Bochu, J. J. Aubert, J. C. Joubert, and M. Marezio, *J. Solid State Chem.* **24,** 245 (1978).
17. C. C. Pham, J. Choisnet, and B. Raveau, *Bull. Acad. Roy. Belge Sci.* **61,** 473 (1975).
18. A. A. Awadalla and B. M. Gatehouse, *J. Solid State Chem.* **23,** 349 (1978).
19. B. Bochu, M. N. Deschizeaux, J. C. Joubert, A. Collomb, J. Chenavas, and M. Marezio, *J. Solid State Chem.* **29,** 291 (1979).